Chemosphere 201 (2018) 790–798

Contents lists available at ScienceDirect

Chemosphere

journal homepage: www.elsevier.com/locate/chemosphere

Oxidation of reduced daughter products from 2,4-dinitroanisole (DNAN) by Mn(IV) and Fe(III) oxides

Raju Khatiwada [a], Christopher Olivares [b], Leif Abrell [a, c], Robert A. Root [a], Reyes Sierra-Alvarez [b], James A. Field [b], Jon Chorover [a, c, *]

[a] Department of Soil, Water and Environmental Science, University of Arizona, Tucson, AZ, USA
[b] Department of Chemical and Environmental Engineering, University of Arizona, Tucson, AZ, USA
[c] Arizona Laboratory for Emerging Contaminants, University of Arizona, Tucson, AZ, USA

HIGHLIGHTS

- Insensitive munition compound DNAN is resistant to oxidation by soil minerals.
- DNAN reduced daughter products, MENA and DAAN, are oxidized by birnessite.
- DAAN can be oxidized by either ferrihydrite or birnessite.
- MENA reacted with birnessite releases N to nitrite.

GRAPHICAL ABSTRACT

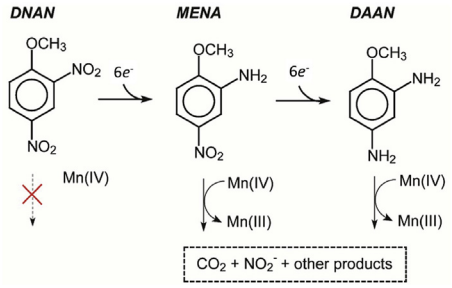

ARTICLE INFO

Article history:
Received 31 October 2017
Received in revised form
21 February 2018
Accepted 3 March 2018
Available online 5 March 2018

Handling Editor: W. Mitch

Keywords:
Insensitive munitions compound (IMC)
2,4-Dinitroanisole (DNAN)
2-methoxy-5-nitro aniline (MENA)
2,4-Diaminoanisole (DAAN)
Ferrihydrite
Birnessite

ABSTRACT

Abiotic transformation of anthropogenic compounds by redox-active metal oxides affects contaminant fate in soil. The capacity of birnessite and ferrihydrite to oxidize the insensitive munitions compound, 2,4-dinitroanisol (DNAN), and its amine-containing daughter products, 2-methoxy-5-nitro aniline (MENA) and 2,4-diaminoanisole (DAAN), was studied in stirred reactors at controlled pH (7.0). Aqueous suspensions were reacted at metal oxide solid to solution mass ratios (SSR) of 0.15, 1.5 and 15 g kg^{-1} and solutions were analyzed after 0–3 h by high performance liquid chromatography coupled with photodiode array or mass spectrometry detection. Results indicate that DNAN was resistant to oxidation by birnessite and ferrihydrite. Ferrihydrite did not oxidize MENA, but MENA was susceptible to rapid oxidation by birnessite, with nitrogen largely mineralized to nitrite. This is the first report on mineralization of nonphenolic aromatics and the release of mineralized N from aromatic amines following reaction with birnessite. DAAN was oxidized by both solids, but *ca.* ten times higher rate was observed with birnessite as compared to ferrihydrite at an SSR of 1.5 g kg^{-1}. At 15 g kg^{-1} SSR, DAAN was removed from solution within 5 min of reaction with birnessite. $CO_{2(g)}$ evolution experiments indicate mineralization of 15 and 12% of the carbon associated with MENA and DAAN, respectively, under oxic conditions with birnessite at SSR of 15 g kg^{-1}. The results taken as a whole indicate that initial reductive (bio)transformation products of DNAN are readily oxidized by birnessite. The oxidizability of the reduced DNAN products was increased with progressive (bio)reduction as reflected by impacts on the oxidation rate.

* Corresponding author. Department of Soil, Water and Environmental Science, University of Arizona, Tucson, AZ, USA
E-mail address: chorover@email.arizona.edu (J. Chorover).

https://doi.org/10.1016/j.chemosphere.2018.03.020
0045-6535/

1. Introduction

The U.S. Department of Defense (DoD) is evaluating new and safer alternatives to traditional munitions compounds. The insensitive munitions compound (IMC), 2,4-dinitroanisole (DNAN), is one of those being testing to replace the traditional munitions compound, 2,4,6-trinitrotoulene (TNT), because it exhibits lower susceptibility to unintended detonation by shock and heat (Walsh et al., 2013). However, upon detonation, a substantial mass fraction of free product often remains unaltered and DNAN is subsequently passively released into the environment during residue dissolution (Morley et al., 2006; Taylor et al., 2009). The fate and transport of these compounds in soil systems remains poorly understood. Furthermore, recent studies have indicated that, under anoxic soil conditions, DNAN is subjected to microbially-mediated or mineral-surface-catalyzed reduction to form potentially toxic aromatic amine daughter products 2-methoxy-5-nitro aniline (MENA) and 2,4-diaminoanisole (DAAN) (Liang et al., 2013; Hawari et al., 2015, Olivares et al., 2013, 2016a, 2016b). Despite this, there has been very limited study on the fate of these daughter compounds in soil. These potentially toxic aromatic amines that form during different stages of transformation of the parent compound DNAN may also pose environmental threats to the soil and aquatic systems.

Electron transfer reactions at soil mineral surfaces play an important role in the abiotic transformation of organic environmental contaminants (Laha and Luthy, 1990; Pizzigallo et al., 1998; Majcher et al., 2000; Li et al., 2003). Iron-bearing minerals are abundant and have been shown to transform xenobiotics, including explosive compounds (Hofstetter et al., 1999; Boparai et al., 2010; Ou et al., 2015). Despite their lower mass concentration in soils, manganese (III, IV) oxide minerals, such as birnessite ($[Na,Ca,Mn^{2+}][Mn^{3+},Mn^{4+}]_7O_{14}\cdot 2.8H_2O$) have been found to be capable of oxidizing organic compounds including phenolics like catechol, hydroquinone, resorcinol, aniline and its derivatives (Laha and Luthy, 1990; Klausen et al., 1997; Pizzigallo et al., 1998; Majcher et al., 2000; Colon et al., 2002; Li et al., 2003; Chien et al., 2009), eventually leading to reactive intermediates that may undergo polymerization or partial mineralization to $CO_{2(g)}$ (Majcher et al., 2000; Kang et al., 2006; Li et al., 2012). The inherent oxidizing or reducing capability of minerals must be resolved to predict the fate of novel IMCs in soils. Toward that goal, we chose two mineral models (i) birnessite and (ii) ferrihydrite ($Fe^{III}_2O_3\cdot 0.5H_2O$) to better understand their reactivity toward the parent compound DNAN and its daughter products MENA and DAAN. These minerals are known for their surface reactivity and are commonly found in soils and sediments (Essington and Vergeer, 2015).

Birnessite (denoted from here simply as $MnO_{2(s)}$) is a common representative of Mn(III, IV) containing secondary mineral forms produced as a result of primary mineral weathering in soils. It exhibits both permanent and pH-dependent surface charge, the former as a result of Mn(IV) vacancy sites in the crystal structure, and the latter because of proton adsorption-desorption on Mn-OH surface functional groups (Essington, 2015). Synthetic "acid birnessite" prepared from reduction of potassium permanganate has been widely used as surrogate for naturally-occurring biogenic birnessite (Chorover and Amistadi, 2001; Villalobos et al., 2003). Ferrihydrite is a poorly-crystalline and highly-reactive hydrous Fe(III) oxide that serves as an important sink for contaminant metals and an oxidizing agent for some organic compounds (Waychunas et al., 2005). The high surface-reactivity of ferrihydrite includes the capacity for either reductive or oxidative transformation, wherein it promotes Fe(II)-sorbate-induced reduction of DNAN (Niedzwiecka and Finneran, 2015) or the surface Fe(III)-induced oxidative transformation of aromatic amine biotransformation products.

The objectives of the study were to (i) assess the oxidation potential of IMCs and their daughter products by birnessite and ferrihydrite, and (ii) identify the inorganic oxidation products. The ability of birnessite and ferrihydrite to abiotically transform the IMC parent compound DNAN in comparison with its daughter products, MENA and DAAN, was studied under well-controlled laboratory conditions.

2. Materials and methods

All chemicals used were ACS reagent grade or better, and all solutions were prepared from ultrapure (Barnstead nanopure, 18.2 MΩ) water. The details of mineral synthesis and characterization methods, including mineral purity, specific surface area and particle size distribution, are described in Supplementary Information (section A.1).

2.1. IMCs and daughter products

2,4-dinitroanisole (DNAN; CAS #119-27-7, 98% purity) was purchased from Alfa Aesar (Ward Hill, MA). 2-methoxy-5-nitroaniline (MENA; CAS #99-59-2, 98% purity) and 2,4 diaminoanisole (DAAN; CAS #615-05-4, 99.6% purity) were purchased from Sigma–Aldrich (St Louis, MO). The physico-chemical properties of the compounds are listed (Table A.1).

2.2. Time series kinetic experiments

Time series experiments were conducted to quantify the abiotic transformation potential of IMCs by birnessite and ferrihydrite at solid to solution ratios (SSR) of 0.15, 1.5 and 15 g kg^{-1}. One hundred mL of 1 mM DNAN, MENA or DAAN solution (in 10 mM NaCl as background electrolyte) at pH 7.0 were placed in a reactor with a magnetic stirrer and the appropriate dry mass of birnessite or ferrihydrite was added with rapid mixing to initiate the reaction at the desired SSR ratios. The pH was controlled at 7.0 by titration of 10 mM HCl or NaOH throughout the reaction. Samples were taken at time intervals of 0, 5, 10, 20, 40, 60 and 180 min for birnessite reaction and at 0, 15, 30, 60 and 180 min for ferrihydrite. Solids were separated via centrifugation at 41,500 g for 5 min using an Eppendorf 5417C bench top micro-centrifuge. The supernatant solution was analyzed for equilibrium concentration of IMCs using ultra high performance liquid chromatography with photodiode array detection (UHPLC-PDA) for target compounds. All time series experiments were conducted under oxic conditions (in equilibrium with atmospheric air) at 25 °C. Surface-area normalized pseudo first order rate coefficients [for oxidation kinetics were determined from the magnitude of the slope of the regression line resulting from plotting the log of normalized reactant concentration (C_t/C_0) vs time (h) for first three data points, where C_t is the concentration of compound at time t, and C_0 is the initial concentration of the compound at time zero, normalized to specific surface area.

2.3. CO_2 evolution experiments

A separate set of experiments was conducted in closed serum bottles to measure the extent to which IMC and daughter product oxidation resulted in compound mineralization to $CO_{2(g)}$. These experiments were carried out in closed serum bottles in 10 mM NaCl background and initial pH 7.0, at 25 °C. Forty mL of 1 mM DNAN, MENA or DAAN solution were added to 0.6 g mineral in a serum bottle (Volume = 155.5 cm^3) in triplicate at SSR of 15 g kg^{-1}. The samples were allowed to react for 3 h, and $CO_{2(g)}$ released to the headspace was measured using gas chromatography after

acidification (pH 2) of the solution with 0.1 M HCl. Total CO_2 production reported here accounts for headspace $CO_{2(g)}$, dissolved CO_2 and carbonic acid, which were calculated from gas phase concentrations using Henry's law. Experimental controls included IMC-free and mineral-free reactors to account for background CO_2 degassing from solution and surfaces.

Effects of presence and absence of O_2 during this reaction was also tested with MENA. MENA conversion to $CO_{2(g)}$ was quantified using O_2 headspace partial pressures of 0, 5 and 20 with He as the second gas. Samples were reacted for 3 h, and $CO_{2(g)}$ release to the headspace was measured by gas chromatograph after acidification of the solution.

2.4. Inorganic N formation

To measure production of inorganic nitrogen species from organic contaminant oxidation, a separate set of time series experiments were conducted at 15 g kg^{-1} SSR in deionized water, in the absence of added background electrolyte to avoid analytical interference from Na^+ and Cl^- in quantification of inorganic N species. Samples were collected as a function of reaction time and analyzed for dissolved NH_4^+, NO_2^- and NO_3^-.

2.5. Aqueous chemical analyses

Concentrations of DNAN, MENA and DAAN in liquid samples were analyzed using UHPLC-PDA (Agilent 1200 Infinity Series, Santa Clara, CA). Five μL of sample were injected onto RSLC E2 Acclaim Explosives column (2.1 × 100 mm, particle size 2.2 μm; Thermo Scientific, Waltham, MA, USA) at room temperature and separated using a 40/60% methanol/water mobile phase at 0.25 mL min-1 over a 15 min run time. DNAN (retention time [RT] = 7 min) was quantified on the basis of peak area by absorption at wavelength 300 nm. MENA (RT = 5 min) and DAAN (RT = 2.0 min) were quantified at 254 nm.

Aqueous solutions from across the time series for the 15 g kg^{-1} SSR birnessite experiments were also analyzed using an Dionex Ultimate 3000 UHPLC coupled to a Q Exactive Focus Hybrid Quadrupole-Orbitrap mass spectrometer (Thermo Scientific, Waltham, MA, USA) to detect organic reaction products. Five μL of sample were injected onto an RSLC E2 Acclaim Explosives column (2.1 × 100 mm, particle size 2.2 μm; Thermo Scientific, Waltham, MA, USA) at 25 °C and separated isocratically using a 40/60% methanol/water mobile phase at 0.25 mL min^{-1} over a 15 min run time. Reaction products were detected using electrospray ionization (ESI) high resolution mass spectrometry in both positive and negative ion modes.

Inorganic nitrogen species, NH_4^+, NO_2^-, and NO_3^- potentially released during oxidation of the IMC and daughter products were measured using ion chromatography (IC) with conductivity detection; ammonium was measured using a Dionex ICS-1000 equipped with a CS-16 column (Sunnyvale, CA) and anions were measured with a Dionex LC 20 with an Ionpac AS11 column (Sunnyvale, CA). The eluent flow rates for anion and cation analysis were both 1.0 mL min^{-1}. Total solution phase manganese was measured using an Elan DRC-II inductively coupled plasma mass spectrometer (ICP-MS) (Perkin Elmer, Waltham, MA, USA). Headspace $CO_{2(g)}$ was analyzed by injecting a 10 μL headspace sample into an Agilent Technologies 7890A GC (Santa Clara, CA) equipped with an J&W 113-4332 GS-DASPRO column (30 × 0.320 mm) using air tight Hamilton needles. Gas was heated to 200 °C at 14.68 psi with influent He gas flow of 2504 mL min^{-1} and signal was measured using a total carbon detector at a data rate of 50 Hz. Total CO_2 production reported here accounts for headspace $CO_{2(g)}$, dissolved CO_2 and carbonic acid, which were calculated from gas phase concentrations using Henry's law.

2.6. Solid phase analyses

Bragg reflections from XRD were collected for freeze dried powders of the control- and MENA-reacted birnessite in transmission mode on beamline 11-3 at the Stanford Synchrotron Radiation Lightsource (SSRL) at fixed X-ray energy of 12.7 keV (0.9765 Å) and calibrated to a LaB_6 standard. Analysis of the diffractograms for peak position (°2θ and d-spacing [Å]), height, full width at half maximum (FWHM), and peak area was performed using X'Pert HighScore Plus software (PANalytical).

Selected reacted and unreacted birnessite samples were analyzed by X-ray photoelectron spectroscopy (XPS) to detect changes in Mn oxidation state using a Kratos Axis 165 Ultra X-ray photoelectron spectrometer (Kratos Analytical Ltd, UK). The XPS employed an Al monochromatic source and an array of eight channeltron electron dmultipliers for detection. The sample chamber was continuously purged with $He_{(g)}$, and Mn 3s spectra were collected at high resolution to identify changes in Mn redox speciation induced by reaction.

3. Results

3.1. Reaction of DNAN, MENA and DAAN with ferrihydrite

The reactivity of DNAN, MENA and DAAN was tested with ferrihydrite at a SSR of 0.15, 1.5 and 15.0 g kg^{-1}. There was no reaction of DNAN and MENA with ferrihydrite within the 3 h reaction time for all of the solid phase concentrations tested (Table 1). However, DAAN was reactive with ferrihydrite at 1.5 and 15 g kg^{-1} SSR (Table 1). There was an initial decline in DAAN concentration; however, the reaction seems to stall and the amount of DAAN in solution reaches a near-steady value after 60 min for 1.5 g kg^{-1} SSR. However, for 15 g kg^{-1} SSR, there was gradual decline in DAAN concentration up to 3 h reaction time. The plots for ln (C_t/C_0) vs time (h) with the linear regression fits for DAAN with ferrihydrite are shown in Fig. A.1. Surface area normalized pseudo first order rate constants were similar for DAAN at various concentrations used; however faster reaction rate (~20 fold) was seen for specific surface area normalized ferrihydrite at 15 g kg^{-1} SSR compared to 1.5 g kg^{-1} SSR higher concentration (Table 1).

3.2. Oxidation of DNAN, MENA and DAAN by birnessite

There was no detectable reaction of DNAN with birnessite under the experimental conditions tested over a 3 h period (Table 1). However, DNAN daughter products were transformed by birnessite oxidation within 3 h for MENA and within 5 min for DAAN at a SSR of 15 g kg^{-1} (Fig. 1A), corresponding to first order rate constants of 4.81 and ≥ 90.5 h^{-1}, respectively (Table 1). At a lower SSR of 1.5 g kg^{-1} with birnessite (Fig. 1B), the first order reaction produced rate constants of 0.637 and 2.582 h^{-1} for MENA and DAAN, respectively, (Table 1). The plots for ln (C_t/C_0) vs time (h) with the linear regression fits for MENA and DAAN with birnessite are shown in Figs. A.2 and A.3 respectively. There was complete loss of MENA (m/z 169.15) after the reaction with birnessite at 15 g kg^{-1} SSR birnessite as evident from mass spec data as well (Fig. A.4). A direct comparison for the oxidation of DAAN by birnessite and ferrihydrite at an SSR of 1.5 g kg^{-1} (Table 1) indicates a stark contrast in the ability of birnessite and ferrihydrite to oxidize the daughter products of DNAN. Birnessite oxidized both MENA and DAAN; whereas only DAAN oxidation was detected with ferrihydrite (Table 1). Furthermore, the rate of DAAN oxidation was five-fold faster with birnessite compared to ferrihydrite when each

Table 1
Mineral-surface area normalized pseudo first-order rate constants (k) of IMC and daughter product oxidation by birnessite and ferrihydrite supplied at various solid to solution ratios.

Mineral Surface	SSA[a] ($m^2\ g^{-1}$)	SSR[b] ($g\ kg^{-1}$)	Total SA ($m^2\ kg^{-1}$)	Normalized Pseudo 1st Order Rate Constants (k, $h^{-1}\ m^{-2}$)		
				DNAN	MENA	DAAN
Birnessite	83.8					
		0.15	12.59	*bd*[c]	0.003 (0.93)	0.097 (0.99)
		1.50	125.9	*bd*	0.005 (0.92)	0.021 (0.99)
		15.0	1259	*bd*	0.004 (0.90)	0.072 (1.00)
				Mean:	**0.004 ± 0.001**	**0.063 ± 0.038**
Ferrihydrite	155.0					
		0.15	23.25	*bd*	*bd*	ND
		1.50	232.5	*bd*	*bd*	0.002 (0.74)
		15.0	2325	*bd*	*bd*	0.039 (0.99)
				Mean:	***bd***	**0.021 ± 0.026**

[a] SSA = specific surface area.
[b] SSR = solids solution ratio.
[c] *bd* indicates *below detection*, i.e., no measurable reaction at 3 h; in the case of DNAN plus birnessite and DNAN/MENA plus ferrihydrite, no reactions were observed. † Values in parentheses are R^2 values for the regression fit. ** Value estimated from the slope of first two data points only, because the concentration reached zero at 5 min. The rate may be higher than the estimated rate as the actual reaction end-point might be less than 5 min, here denoted by ≥ in the table. N/A = not applicable. ND = no data.

was supplied at 1.5 g kg^{-1} SSR (Table 1). Plateauing of DAAN concentration after 60 min was observed with ferrihydrite at an SSR of 1.5 g kg^{-1} indicating system became limited in oxidant (Fig. 1). Surface area normalized pseudo first order rate constants were similar for MENA and DAAN at various concentrations used (Table 1).

The number of nitro- and amino-groups on the compound molecule highly impacted the oxidation rate by birnessite. The IMC parent compound, DNAN, with two nitro-groups was not oxidized. However, the reduced daughter products were oxidized and the rates increased as the number of amino-groups increased and nitro-groups decreased. DAAN with two amino-groups was oxidized five-fold faster than MENA which has one-amino and one-nitro group (Table 1). Even at the lowest tested SSR of 0.15 g kg^{-1}, the first order rate constant for DAAN oxidation by birnessite was 1.216 h^{-1} but the reaction then plateaued after 40 min (Fig. 1C) indicating depletion of reactive oxidant. Conversely, there was no measurable MENA oxidation over a 3 h period at the lowest SSR value (Table 1).

3.3. Organic reaction products

LC-MS analysis of MENA solutions reacted with birnessite revealed four principal reaction products, all detected in ESI positive mode, with m/z values of 155, 167, 198, and 348, Fig. 2A). In addition to those shown in Fig. 2A, a large peak corresponding to m/z 183 was observed in ESI negative mode, but only for the final (180 min) sample. LC-MS analysis of birnessite-DAAN solutions revealed one product in ESI negative mode at m/z 175, and four products in ESI positive mode, with m/z 273, 275, 305, and 379 (Fig. 2b). Peak areas for all of these compounds were absent from the initial time zero solution, and increased with time following

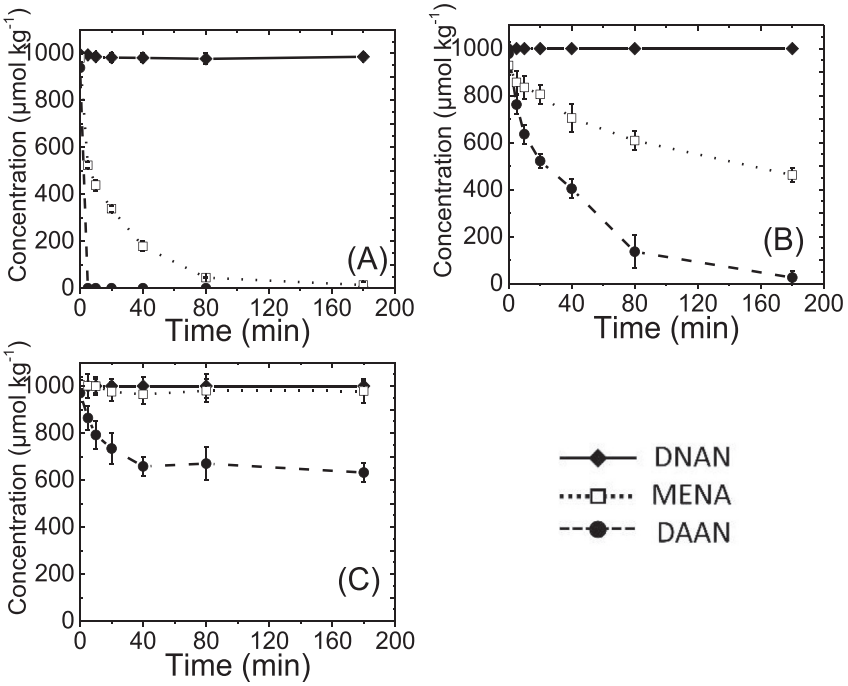

Fig. 1. Transformation of DNAN (◆), MENA (□) and DAAN (●) by birnessite at (A) 15 g kg^{-1}, (B) 1.5 g kg^{-1} and (C) 0.15 g kg^{-1} solid to solution ratio (SSR) at pH 7.0. Error bars representing standard deviations of duplicate measurements are smaller than symbols when not shown.

contact with the water-wetted surface of birnessite (Fig. 2). Detailed structural characterization of these reaction products is ongoing, but several observations are noteworthy in respect to the current study.

First, the product *m/z* values suggest that reaction products are of comparable or higher molecular mass than the MENA and DAAN compounds undergoing oxidation. Hence, there is no evidence of oxidative ring cleavage leading to low molar mass compounds. Rather, these data are consistent with oxidation of substituent groups and potential subsequent oxidative coupling reactions. Second, the peaks at *m/z* 273 and 275 observed following reaction with DAAN, which show steady growth over the 3 h reaction time, are consistent with dimers observed to form during a prior study of anaerobic biotransformation of the parent DNAN. On the basis of that study (Olivares et al., 2016b), these product peaks are putatively assigned to 3.3′-diamino-4.4′dimethoxy-azobenzene ($C_{14}H_{16}N_4O_2$) and 3.3′-diamino-4.4′dimethoxy-hydrazobenzene ($C_{14}H_{18}N_4O_2$), respectively. Laha and Luthy (1990) originally reported the dimerization of aniline to form azobenzene and 4-aminodiphenylamine upon surface reaction with MnO_2. These authors attributed the products to the one-electron transfer from aniline to MnO_2, which resulted in the formation of organic cation radicals that then undergo coupling reactions to form the dimer. A similar coupling reaction at $R{-}NH_2^{\bullet}$ groups, is apparent in the case of DAAN, and it helps to explain low N mineralization (i.e., nitrite formation) observed in DAAN relative to MENA (see next section).

3.4. Extent of mineralization

For those conditions showing maximum MENA and DAAN removal (15 g kg^{-1} birnessite), companion experiments were conducted to assess $CO_{2(g)}$ evolution from the reaction. Data show that under oxic conditions (20% O_2), 15% and 12% of the C was mineralized to $CO_{2(g)}$ for MENA and DAAN, respectively (Fig. 3A). Furthermore, the data show that mineralization to $CO_{2(g)}$ was not limited by presence of $O_{2(g)}$, since the fraction of MENA mineralized following reaction with birnessite in a 0.01 M NaCl background was independent of $O_{2(g)}$ partial pressure (Fig. 3A).

In addition to partial mineralization of IMC daughter organic C to $CO_{2(g)}$, the release of organic N to inorganic forms was also observed for both MENA and DAAN reaction with birnessite, albeit to different extents. For MENA, results indicate nitrite (NO_2^-) as the dominant N degradation product, with *ca.* 95% of MENA nitrogen recovered in this inorganic form following 3 h of oxidation by birnessite (Fig. 3B). A smaller yield of NO_2^- was observed for DAAN, equating to *ca.* 15% of total DAAN-N (e.g., compare Figs. A.2 and A.3). Much less NH_4^+-N (<2%) and NO_3-N (<5%) and no N_2-N were detected as a product of either MENA or DAAN oxidation (Figs. A.5 and A.6).

The yield of soluble Mn(II) was much less than that calculated based on stoichiometric conversion of birnessite Mn(IV) to soluble Mn(II) during reaction with IMC daughter products. For MENA and DAAN, only 34.5 μg kg^{-1} and 782.4 μg kg^{-1} of Mn(II) were recovered from solution respectively at the end of 3-h reaction. These measured values are more than three orders of magnitude lower than the values of 935 and 988 mg kg^{-1} Mn(II) calculated for complete stoichiometric conversion of MENA and DAAN to CO_2 and NO_2^- or N_2, respectively. Calculations of $Mn^{2+}{}_{(aq)}$ generated from 12% (MENA) and 15% (DAAN) conversion to mineralized products, as measured in the experiments, also give concentrations *ca.* 4000 and 152 times higher for Mn(II) concentrations in solution than those measured. This indicates a solid-phase fate for the reduced Mn.

3.5. Transformation of birnessite based on X-ray diffraction (XRD)

The unreacted birnessite showed the expected Bragg reflections including (001) at 7.294 Å, (002) at 3.633 Å, and the strongly asymmetrical (220/110) and (310/020) peaks at 2.468 Å and 1.424 Å respectively (Fig. 4A). The MENA-reacted birnessite showed no change in the (001) peak position, height or FWHM. The (002) and (220/110) peak showed distortions with the (002) reflection 0.017 Å closer, 11% lower in height, but at the same full width at half maximum (FWHM); the (220/110) reflection was 0.009 Å longer, no change in height, and a FWHM at 50% the value of the unreacted birnessite. The (020) showed no change in d-spacing, but a 20% decrease in the FWHM.

3.6. Transformation of birnessite based on X-ray photoelectron spectroscopy (XPS)

High resolution Mn3s spectra for birnessite reveal detectable changes in Mn oxidation state following reaction of MENA (Fig. 4B) with 15 g kg^{-1} SSR birnessite. The magnitude of peak splitting for Mn3s high resolution spectra is diagnostic for the oxidation state of Mn (Cerrato et al., 2010). Unreacted birnessite shows a binding energy difference between Mn3s splitting multiplex of 4.5 eV, consistent with predominance of Mn(IV) oxidation state, whereas

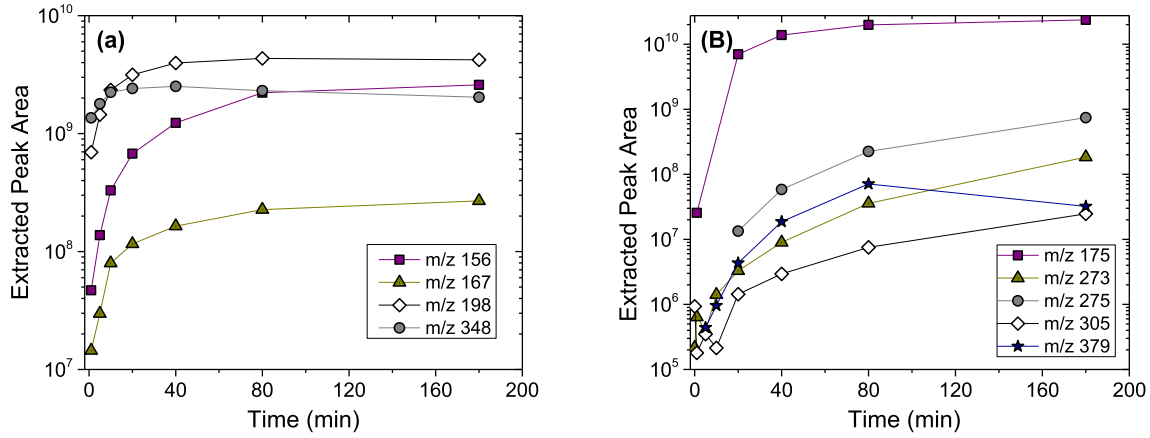

Fig. 2. Time series of extracted mass chromatogram peak areas for organic products deriving from (A) MENA and (B) DAAN reaction with birnessite at 15 g kg^{-1} SSR. All *m/z* values for MENA experiment (A) correspond to the negative charged ions (i.e., measured in ESI negative mode), and all *m/z* values for DAAN (B) correspond to the positive charged ions (i.e., measured in ESI positive mode) except for *m/z* 175, which was measured in ESI negative mode.

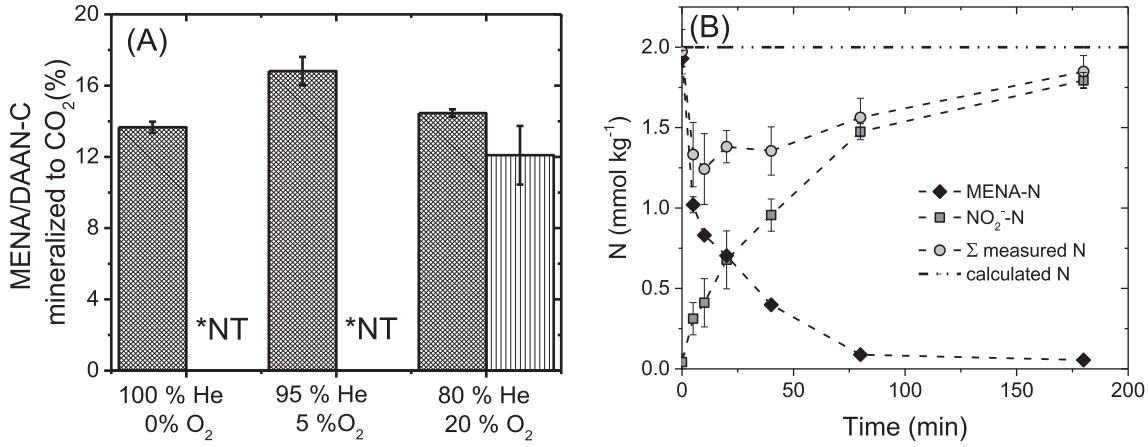

Fig. 3. (A) The percent conversion of MENA (cross-hatched) or DAAN-C (vertical lines) to $CO_{2(g)}$ during incubations with birnessite 15 g kg^{-1} solid to solution ratio over a 3 h incubation period with 0, 5 and 20% O_2 in the headspace. DAAN $CO_{2(g)}$ emission was tested with 20% O_2 in the headspace only, *NT = not tested; (B) Nitrite recovery from MENA birnessite reaction at 15 g kg^{-1} solid to solution ratio at pH 7.0.

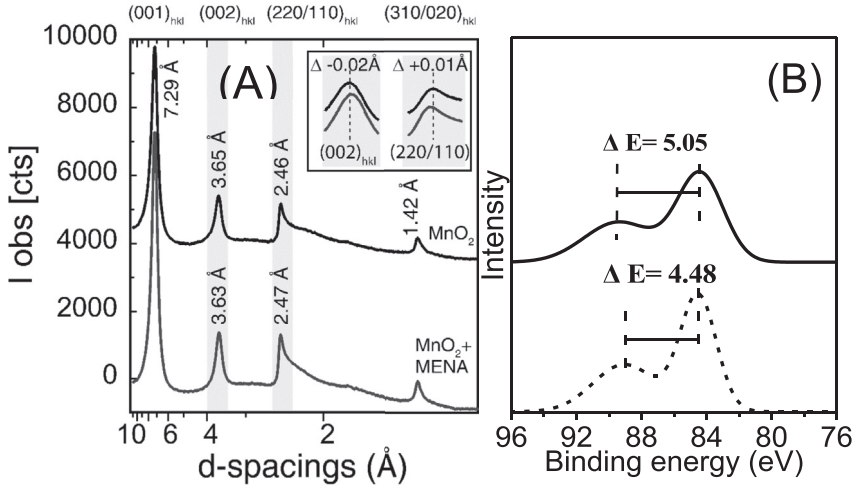

Fig. 4. (A) XRD pattern of birnessite (MnO_2) and its transformation product after treatment with 1 mM MENA at pH 7. Peaks are labeled with the assigned diffracting planes (*hkl*) and d-spacing (Å). Insets are the (002) and (220/110) peaks to show the offset of the MENA reacted birnessite. (B) High resolution Mn 3s scan for unreacted and post MENA reacted birnessite (15 g kg^{-1}) at pH 7.0. The solid line is birnessite + MENA, the dashed line is only birnesite. The increase in binding energy difference indicates reductive dissolution of birnessite and incorporation of reduced Mn forms back to the solids. Background electrolyte = 10 mM NaCl.

following 3 h reaction with MENA, the binding energy difference between Mn3s splitting multiplex shifts to 5.05, indicating reduction of a portion of birnessite Mn (IV) to a mixture of Mn (II and III). The Mn shift towards higher binding energy is consistent with the low aqueous recovery of Mn discussed above, and suggests that reductive transformation of birnessite upon reaction with IMC daughter products results in subsequent re-incorporation of reduced Mn into the solids.

4. Discussion

The metal oxides birnessite and ferrihydrite were tested for their reactivity with DNAN and its daughter products MENA and DAAN. The results indicate a strong dependence on mineral type and solid concentration. The parent compound DNAN was found to be stable and non-reactive with both birnessite and ferrihydrite. DNAN structure has two nitro groups in the ortho and para positions (Table A.1). The nitro groups in DNAN structure have a strong electronegativity resulting from the combined action of two electron withdrawing oxygen atoms bonded to the partially negative nitrogen atom (Ju and Parales, 2010). The nitro group strongly inhibits electrophilic substitution in the aromatic ring (Niedzwiecka and Finneran, 2015). Under reducing conditions, DNAN is found to undergo regioselective reduction to MENA, which then gets further reduced further to DAAN (Perreault et al., 2012; Olivares et al., 2013, 2016a; Hawari et al., 2015). In MENA, the ortho nitro group is replaced by an amine (-NH_2) (Table A.1). The amine substituent acts as a nucleophile, where an active lone pair of electrons on the N atom are attracted to reaction with electrophilic Mn(IV) in birnessite (Colon et al., 2002; Li et al., 2003). The presence of two amine groups in DAAN (Table A.1) is, therefore, consistent with its faster oxidation rate by birnessite and even ferrihydrite. There have been some studies regarding oxidation of compounds like anilines and hydroquinone by ferrihydrite (Pizzigallo et al., 1998; Anschutz and Penn, 2005; Borch et al., 2005). So, DAAN may undergo abiotic oxidation by ferryhidrite. Both of the oxides (ferrihydrite and birnessite) are kinetically stable under oxic conditions. The reduction potential of ferrihydrite is approximately 0.0 eV, whereas birnessite has reduction potential of 0.6 eV (Essington, 2015; Salter-Blanc et al., 2016), thus making birnessite a stronger oxidizing agent

than ferrihydrite.

Pizzigallo et al. (1998) have previously compared the efficacy Mn(IV) and Fe(III) oxides for oxidation of the anilines 4-chloroaniline (4-CA), 3,4-dichloroaniline (3,4-DCA) and 3,5-DCA. At pH 6-7, oxidation of only 4-CA was observed, and only with Mn oxide, with no oxidation by Fe oxide. At pH 5, both 3,4-DCA and 4-CA were 65% oxidized by Mn oxide, whereas less than 5% oxidation occurred with Fe oxide; and at pH 4, 3,4-DCA, 3,5-DCA and 4-CA were completely (or nearly completely) oxidized by Mn oxide, whereas 5–15% oxidation was observed with Fe oxide. Products of oxidation were only identified when birnessite was used. Electron withdrawing groups (EWG) such as the nitro groups in MENA and DNAN increase the standard reduction potential and make the anilines less susceptible to oxidation whereas electron donating groups such as a *p*-methoxy group decrease the standard reduction potential and render the compounds more susceptible to oxidation (Laha and Luthy, 1990; Klausen et al., 1997). A kinetic rate study showed a *ca.* 1000-fold slower oxidation rate for *p*-nitroaniline as compared to aniline upon reaction with MnO_2 at pH 4 (Laha and Luthy, 1990). In contrast, oxidation of *p*-methoxyaniline was 3000-fold faster than aniline. Therefore, the progressive (bio) reduction of DNAN is expected to increase the oxidizability of the molecule, and this was reflected in the present study in terms of higher rate of oxidation.

Previous studies with non-phenolic aromatic amines such as aniline, *p*-methoxyaniline, nitroaniline and dichloroaniline indicate that the principal reaction with MnO_2 is a one-electron oxidation to a cation radical, and subsequent coupling to form azo-dimers and diphenylamines and oligomers connected by N=N and C-N bonds (Laha and Luthy, 1990; Pizzigallo et al., 1998). Eventually these intermediates become polymerized as evidenced from the formation of oligomers and irreversible bound residue due to reaction of anilines with Mn in soil (Li et al., 2003).

A unique finding in this study was that nonphenolic aromatic amines can become partially mineralized to $CO_{2(g)}$, with yields of $CO_{2(g)}$ ranging from 12 to 15%. The extent of the yield would suggest that the CO_2 was formed from one of seven C atoms in the MENA or DAAN molecule, probably that of the methoxy group, since evidence of ring cleavage is lacking in the LC-MS data. The oxidation of methoxybenzenes by peroxidases via cation radical causes a quinone to form with the simultaneous releases of a methanol (Kersten et al., 1990). A second unique finding is the high yield of NO_2^- formed from the oxidation of MENA by birnessite accounting for nearly all of the N in MENA. Release of N from aromatic amines has never been described previously in reactions involving metal oxides. The fact that NO_2^- is the main mineralized product observed indicates that at least half of the N in MENA (corresponding to the amine group) became oxidized. Mineralization of the daughter products to $CO_{2(g)}$ and $NO_{2(aq)}^-$ (the latter in the case of MENA) indicates partial mineralization. Mineralization of nonphenolic-aromatic amines during reaction with birnessite has never been described before. While it is well established that the carbon in phenolic compounds becomes partially mineralized during oxidation with birnessite, the major reaction is polymerization (Majcher et al., 2000; Li et al., 2012). We were able to recover only *ca.* 15% CO_2 from birnessite MENA/DAAN reactions. The oxidant demand in each case of coupling for MENA and DAAN is much lower than that required for the full mineralization reaction. The rapid loss of daughter products with birnessite thus could also be attributed to formation of coupling products. The mass spec data showed complete loss of MENA (*m*/*z* 169.15) after the reaction with birnessite at 15 g kg^{-1} SSR birnessite. The oxidative transformation of MENA could result in mineralization or oxidative coupling as observed by others for other intermediates of TNT(Kang et al., 2006). High resolution MS spectra collected from *m*/*z* 35–1000 Da show more transformation products below 200 Da as observed in mass spec. The most dominant masses were *m*/*z* 158.0059, 116.9783, 130.0099. Masses on higher side were seen up to *m*/*z* 600 Da but their relative abundance was very low. The peaks with various masses might be due to possible ring cleavage or release of substituents as observed by other researchers for contaminants reaction with birnessite (Majcher et al., 2000; Kang et al., 2006, 2008; Nyanhongo et al., 2006).

Incomplete mineralization leading to polymerization forming diphenylamine and related coupling products can be considered as the major route of transformation for MENA with birnessite. Alternatively, complete mineralization of MENA by birnessite to CO_2 and NO_2^- could be minor pathway for the reaction, yielding Mn(II) or Mn(III). The equilibrium reaction for each scenario with MENA as model example can be written as:

$$18\ MnO_2\ (\text{birnessite}) + C_7H_8N_2O_3(\text{MENA}) + 34\ H^+ \leftrightarrow 18\ Mn^{2+} + 7CO_{2(g)} + 2\ NO_2^- + 21H_2O \quad (1)$$

$$36\ MnO_2(s) + C_7H_8N_2O_3(\text{MENA}) + 106\ H^+ \leftrightarrow 36\ Mn^{3+} + 7CO_{2(g)} + 2\ NO_2^- + 57H_2O \quad (2)$$

$$2\ MnO_2(s) + 2\ C_7H_8N_2O_3\ (\text{MENA}) + 3\ H^+ \rightarrow 2\ Mn^{3+} + C_{12}H_{11}N\ (\text{diphenylamine}) + 2CO_{2(g)} + 3\ NO_2^- \quad (3)$$

$$2\ MnO_2(s) + 2C_7H_8N_2O_3(\text{MENA}) + 6\ H^+ \rightarrow 2\ Mn^{3+} + C_{14}H_{14}N_4O_6(\text{diphenylamine}) + 4H_2O \quad (4)$$

Although much lower aqueous Mn values are expected for the polymerization routes, measured values of Mn in solution were substantially lower than those predicted by these reactions. Aqueous Mn was 0.31% of that calculated for Eq. (3) and 0.31% of that calculated for Eq. (4), and 0.04% of that calculated for Eq. (1).

The XRD reflections in the control and reacted birnessite are broad, indicating poor crystallinity and/or nano-particulate crystallites. The asymmetry of the peaks is due to turbostratic stacking disorder. The ratio of the (220/110) to the (310/020) reflections is $\sqrt{3}$, indicating hexagonal layer symmetry, which is maintained after reaction with MENA. Additionally, the reflection at 1.42 Å is generally diagnostic of hexagonal layered birnessite (Zhao et al., 2015). The MENA reacted birnessite shows no change in the (001) peak size, position, or shape relative to the control, indicating no distortion of the 10 Å spacing of the layered octahedral sheets. The change in the (002) and (220/110) peaks, −0.017 Å and +0.009 Å respectively, could be due to Jahn-Teller distortion of the octahedrally coordinated $Mn^{(IV)}O_6$ groups (Bargar et al., 2005; Zhu et al., 2010). The slight lengthening and sharpening of the (220/110) peak upon reaction with MENA indicates an increased ordering along the *b*-axis and lengthening along the *a*-axis of the unit cell (Zhao et al., 2015). Hexagonal layered birnessite has about 0.25 cation vacancies per layer in the octahedral sheets that Mn(III) can fill either via comproportionation of Mn(II) and Mn(IV) following a two electron transfer from MENA or DAAN, or via a one electron transfer reaction. Either case results in Mn(III) occupying available vacant sites (Grangeon et al., 2014). The affinity of hexagonal layered birnessite surface vacancies for Mn(II) adsorption and subsequent incorporation of Mn(III) into the sheets would result in the changes observed in the diffraction peaks and offers an

explanation for the low recovery of aqueous phase Mn(II) after reaction with MENA. This scenario is also consistent with the XPS data, which shows a net reduction in Mn oxidation state at the birnessite surface (Essington, 2015). The comproportionation reaction between Mn(II) adsorbed on vacant sites and the surrounding octahedrally-coordinated Mn(IV) in the layer structure to form Mn(III) formation, and the subsequent migration of the Mn(III) into vacancies with an ordered distribution in the birnessite layers has been reported recently (Zhao et al., 2016), and we postulate that a similar process is occurring in our experiments, progressively altering the reactivity of the Mn oxide over time.

5. Conclusions

The results of this study suggest that the replacement of electron withdrawing nitro groups by amino groups increases the susceptibility of IMC molecules to oxidation by naturally occurring metal oxides in soils. This is the first report of C and N mineralization of nonphenolic aromatic amines. The parent compound, DNAN, was found resistant to oxidation by both birnessite and ferrihydrite. The first daughter product MENA, as a result of substitution of one nitro group by amine, was found to be reactive with birnessite but not with ferrihydrite. The second daughter product DAAN, formed as a result of substitution of both the nitro groups by amine, was reactive both with birnessite and ferrihydrite, but birnessite was three-fold more reactive. Metal oxides in soil could play a very important role in remediation of IMCs daughter products in the natural environment.

Acknowledgements

We would like to thank Paul Lee at The Laboratory for Electron Spectroscopy and Surface Analysis (LESSA), The University of Arizona for assistance with XPS data collection. This research was supported by the USA Department of Defense, Strategic Environmental Research and Development Program (SERDP) grant number ER 2221. Portions of this research were carried out at the Stanford Synchrotron Radiation Laboratory (SSRL). Use of the SSRL, SLAC National Accelerator Laboratory, is supported by the U.S. Department of Energy, Office of Science, Office of Basic Energy Sciences under Contract No. DE-AC02-76SF00515.

Appendix A. Supplementary data

Supplementary data related to this article can be found at https://doi.org/10.1016/j.chemosphere.2018.03.020.

References

Anschutz, A.J., Penn, R.L., 2005. Reduction of crystalline iron(III) oxyhydroxides using hydroquinone: influence of phase and particle size. Geochem. Trans. 6, 60–66.
Bargar, J.R., Tebo, B.M., Bergmann, U., Webb, S.M., Glatzel, P., Chiu, V.Q., Villalobos, M., 2005. Biotic and abiotic products of Mn(II) oxidation by spores of the marine Bacillus sp. strain SG-1. Am. Mineral. 90, 143–154.
Boparai, H.K., Comfort, S.D., Satapanajaru, T., Szecsody, J.E., Grossl, P.R., Shea, P.J., 2010. Abiotic transformation of high explosives by freshly precipitated iron minerals in aqueous Fe-II solutions. Chemosphere 79, 865–872.
Borch, T., Inskeep, W.P., Harwood, J.A., Gerlach, R., 2005. Impact of ferrihydrite and anthraquinone-2,6-disulfonate on the reductive transformation of 2,4,6-trinitrotoluene by a gram-positive fermenting bacterium. Environ. Sci. Technol. 39, 7126–7133.
Cerrato, J.M., Hochella Jr., M.F., Knocke, W.R., Dietrich, A.M., Cromer, T.F., 2010. Use of XPS to identify the oxidation state of Mn in solid surfaces of filtration media oxide samples from drinking water treatment plants. Environ. Sci. Technol. 44, 5881–5886.
Chien, S.W.C., Chen, H.L., Wang, M.C., Seshaiah, K., 2009. Oxidative degradation and associated mineralization of catechol, hydroquinone and resorcinol catalyzed by birnessite. Chemosphere 74, 1125–1133.
Chorover, J., Amistadi, M.K., 2001. Reaction of forest floor organic matter at goethite, birnessite and smectite surfaces. Geochem. Cosmochim. Acta 65, 95–109.
Colon, D., Weber, E.J., Baughman, G.L., 2002. Sediment-associated reactions of aromatic amines. 2. QSAR development. Environ. Sci. Technol. 36, 2443–2450.
Essington, M.E., 2015. Soil and Water Chemistry: an Integrative Approach, second ed. CRC Press, Boca Raton, FL.
Essington, M.E., Vergeer, K.A., 2015. Adsorption of antimonate, phosphate, and sulfate by manganese dioxide: competitive effects and surface complexation modeling. Soil Sci. Soc. Am. J. 79, 803–814.
Grangeon, S., Lanson, B., Lanson, M., 2014. Solid-state transformation of nanocrystalline phyllomanganate into tectomanganate: influence of initial layer and interlayer structure. Acta Crystallographica Section B-Structural Science Crystal Engineering and Materials 70, 828–838.
Hawari, J., Monteil-Rivera, F., Perreault, N.N., Halasz, A., Paquet, L., Radovic-Hrapovic, Z., Deschamps, S., Thiboutot, S., Ampleman, G., 2015. Environmental fate of 2,4-dinitroanisole (DNAN) and its reduced products. Chemosphere 119, 16–23.
Hofstetter, T.B., Heijman, C.G., Haderlein, S.B., Holliger, C., Schwarzenbach, R.P., 1999. Complete reduction of TNT and other (poly)nitroaromatic compounds under iron reducing subsurface conditions. Environ. Sci. Technol. 33, 1479–1487.
Ju, K.-S., Parales, R.E., 2010. Nitroaromatic compounds, from synthesis to biodegradation. Microbiol. Mol. Biol. Rev. 74, 250.
Kang, K.-H., Lim, D.-M., Shin, H.-S., 2008. A novel solution for hydroxylated PAHs removal by oxidative coupling reaction using Mn oxide. Water Sci. Technol. 58, 171–178.
Kang, K.H., Lim, D.M., Shin, H., 2006. Oxidative-coupling reaction of TNT reduction products by manganese oxide. Water Res. 40, 903–910.
Kersten, P.J., Kalyanaraman, B., Hammel, K.E., Reinhammar, B., Kirk, T.K., 1990. Comparison of lignin peroxidase,horseradish-peroxidase and laccase in the oxidation of methoxybenzenes. Biochem. J. 268, 475–480.
Klausen, J., Haderlein, S.B., Schwarzenbach, R.P., 1997. Oxidation of substituted anilines by aqueous MnO2: effect of co-solutes on initial and quasi-steady-state kinetics. Environ. Sci. Technol. 31, 2642–2649.
Laha, S., Luthy, R.G., 1990. Oxidation of aniline and other primary aromatic-amines by manganese-dioxide. Environ. Sci. Technol. 24, 363–373.
Li, C., Zhang, B., Ertunc, T., Schaeffer, A., Ji, R., 2012. Birnessite-induced binding of phenolic monomers to soil humic substances and nature of the bound residues. Environ. Sci. Technol. 46, 8843–8850.
Li, H., Lee, L.S., Schulze, D.G., Guest, C.A., 2003. Role of soil manganese in the oxidation of aromatic amines. Environ. Sci. Technol. 37, 2686–2693.
Liang, J., Olivares, C., Field, J.A., Sierra-Alvarez, R., 2013. Microbial toxicity of the insensitive munitions compound, 2,4-dinitroanisole (DNAN), and its aromatic amine metabolites. J. Hazard Mater. 262, 281–287.
Majcher, E.H., Chorover, J., Bollag, J.M., Huang, P.M., 2000. Evolution of CO2 during birnessite-induced oxidation of C-14-labeled catechol. Soil Sci. Soc. Am. J. 64, 157–163.
Morley, M.C., Yamamoto, H., Speitel, G.E., Clausen, J., 2006. Dissolution kinetics of high explosives particles in a saturated sandy soil. J. Contam. Hydrol. 85, 141–158.
Niedzwiecka, J.B., Finneran, K.T., 2015. Combined biological and abiotic reactions with iron and Fe(III)-reducing microorganisms for remediation of explosives and insensitive munitions (IM). Environmental Science-Water Research & Technology 1, 34–39.
Nyanhongo, G.S., Couto, S.R., Guebitz, G.M., 2006. Coupling of 2,4,6-trinitrotoluene (TNT) metabolites onto humic monomers by anew laccase from Trametes modesta. Chemosphere 64, 359–370.
Olivares, C., Liang, J., Abrell, L., Sierra-Alvarez, R., Field, J.A., 2013. Pathways of reductive 2,4-dinitroanisole (DNAN) biotransformation in sludge. Biotechnol. Bioeng. 110, 1595–1604.
Olivares, C.I., Abrell, L., Khatiwada, R., Chorover, J., Sierra-Alvarez, R., Field, J.A., 2016a. (Bio)transformation of 2,4-dinitroanisole (DNAN) in soils. J. Hazard Mater. 304, 214–221.
Olivares, C.I., Sierra-Alvarez, R., Alvarez-Nieto, C., Abrell, L., Chorover, J., Field, J.A., 2016b. Microbial toxicity and characterization of DNAN (bio)transformation product mixtures. Chemosphere 154, 499–506.
Ou, C., Zhang, S., Liu, J., Shen, J., Han, W., Sun, X., Lia, J., Wang, L., 2015. Enhanced reductive transformation of 2,4-dinitroanisole in a anaerobic system: the key role of zero valent iron. Rsc Advances 5, 75195–75203.
Perreault, N.N., Manno, D., Halasz, A., Thiboutot, S., Ampleman, G., Hawari, J., 2012. Aerobic biotransformation of 2,4-dinitroanisole in soil and soil Bacillus sp. Biodegradation 23, 287–295.
Pizzigallo, M.D.R., Ruggiero, P., Crecchio, C., Mascolo, G., 1998. Oxidation of chloroanilines at metal oxide surfaces. J. Agric. Food Chem. 46, 2049–2054.
Salter-Blanc, A.J., Bylaska, E.J., Lyon, M.A., Ness, S.C., Tratnyek, P.G., 2016. Structure-activity relationships for rates of aromatic amine oxidation by manganese dioxide. Environmental Science & Technology 50, 5094–5102.
Taylor, S., Lever, J.H., Fadden, J., Perron, N., Packer, B., 2009. Simulated rainfall-driven dissolution of TNT, tritonal, comp B and octol particles. Chemosphere 75, 1074–1081.
Villalobos, M., Toner, B., Bargar, J., Sposito, G., 2003. Characterization of the manganese oxide produced by *Pseudomonas putida* strain MnB1. Geochem. Cosmochim. Acta 67, 2649–2662.
Walsh, M.R., Walsh, M.E., Taylor, S., Ramsey, C.A., Ringelberg, D.B., Zufelt, J.E., Thiboutot, S., Ampleman, G., Diaz, E., 2013. Characterization of PAX-21 insensitive munition detonation residues. Propellants, Explos. Pyrotech. 38, 399–409.

Waychunas, G.A., Kim, C.S., Banfield, J.F., 2005. Nanoparticulate iron oxide minerals in soils and sediments: unique properties and contaminant scavenging mechanisms. J. Nanoparticle Res. 7, 409–433.
Zhao, H., Liang, X., Yin, H., Liu, F., Tan, W., Qiu, G., Feng, X., 2015. Formation of todorokite from "c-disordered" H+-birnessites: the roles of average manganese oxidation state and interlayer cations. Geochem. Trans. 16.
Zhao, H., Zhu, M., Li, W., Elzinga, E.J., Villalobos, M., Liu, F., Zhang, J., Feng, X., Sparks, D.L., 2016. Redox reactions between Mn(II) and hexagonal birnessite change its layer symmetry. Environmental Science & Technology 50, 1750–1758.
Zhu, M., Ginder-Vogel, M., Parikh, S.J., Feng, X.-H., Sparks, D.L., 2010. Cation effects on the layer structure of biogenic Mn-oxides. Environmental Science & Technology 44, 4465–4471.